Orientation of Piezoelectric Crystals and Acoustic Wave Propagation

Guigen Zhang
Department of Bioengineering, Department of Electrical and Computer Engineering
Institute for Biological Interfaces of Engineering, Clemson University, Clemson, SC 29634
guigen@clemson.edu

Abstract: Surface acoustic wave (SAW) devices are commonly used as wireless filters, resonators and sensors. The confinement of acoustic energy near the surface of a piezoelectric substrate in a SAW sensor makes it highly sensitive for discerning surface perturbation. As sensors, SAW devices have the potential to provide a high-performance sensing platform with capabilities of remote and high-temperature operations. This is very attractive for SAW sensors because dangerous chemical and biological species can be detected in extreme conditions remotely.

Since piezoelectric materials commonly used as SAW substrates are anisotropic, the performance of a SAW device depends on not only the cut angle of its substrate material but also the wave propagation direction. To produce high performance SAW devices, optimal orientations of the crystal cut for the piezoelectric substrate and the SAW propagation are crucial. This work takes advantage of COMSOL Multiphysics computational power to investigate this important problem.

Keywords: Surface acoustic wave, crystal cuts, Euler angles, two-port delay-line sensor.

1. Introduction

SAW based biosensors are MEMS devices in which high frequency acoustic waves travel close to the surface of a piezoelectric substrate. SAW devices are highly sensitive for discerning surface perturbation such as molecular absorption or adsorption and other perturbation. To use a SAW device as a sensor, very often a two-port delay-line configuration is used (Fig.1). In this SAW device, two sets of interdigitated transducers (IDEs) are placed atop a piezoelectric substrate and separated by a distance. The active area between the transmitting and receiving IDEs is often coated with a chemically sensitive layer for molecular absorption or adsorption while the change in wave propagation is characterized for frequency shift and insertion loss.

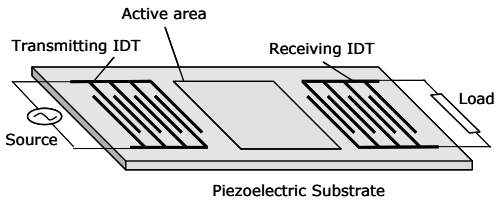

Fig. 1 – Schematic of a two-port delay-line SAW sensor.

2. Constitutive and Wave Equations

A piezoelectric material is often governed by the following constitutive relationships:

$$T = C_E \cdot S - e \cdot E \quad \text{and} \quad d = e \cdot S + \varepsilon \cdot E$$

Where T and S are the stress and strain tensors, E and d are the electric field and displacement vectors, and C_E, e and ε are the stiffness, piezoelectric constant and dielectric matrices of the substrate material, respectively. Considering wave propagation in such a piezoelectric material, we have:

$$\nabla \cdot [e \nabla \phi] + \nabla \cdot [C_E \nabla_s u] - \rho \ddot{u} = 0$$

$$\nabla \cdot [e \nabla_s u] = \nabla \cdot [\varepsilon (\nabla \phi)]$$

Here ρ is the material density, u and $\ddot{u}$ are particle displacement and acceleration, respectively, and φ is the electric potential.

3. Crystal Orientation

Since piezoelectric materials are anisotropic materials, a different orientation of a cut crystal substrate will result in a different set of material properties including the C_E, e and ε matrices, thus affecting the wave propagation characteristics. The selection of a unique crystal cut is often defined by a set of Euler angles (ϕ,θ,ψ). As illustrated in Fig.2, starting from the crystal axises (X, Y, Z), the first Euler angle defines the rotation of ϕ about the Z axis, the second Euler angle defines the rotation of θ about the rotated x' axis, and the third Euler angle defines the rotation of ψ about the rotated z axis to orient the wave propagation in the x

direction. Thus with this Euler angle configuration, the acoustic wave is assumed to be a plane wave in the saggital zx plane, traveling in the x direction. If the wave is polarized in the x direction, the wave is called longitudinal wave; if it is polarized in the z direction, it is shear vertical wave; if it is polarized in the y direction, it is shear horizontal wave. The surface wave is often the coupling of these wave traveling near the surface.

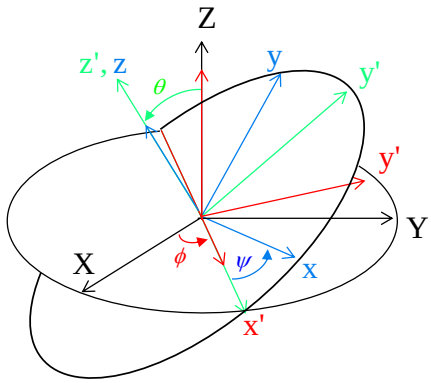

Fig. 2 – Rotation by Euler angles (ϕ,θ, ψ).

With each rotation, two rotation matrices, [a] and [M], can be determined:

$$[a]=\begin{bmatrix} a_{xx} & a_{xy} & a_{xz} \\ a_{yx} & a_{yy} & a_{yz} \\ a_{zx} & a_{zy} & a_{zz} \end{bmatrix}$$

$$[M]=\begin{bmatrix} a_{xx}^2 & a_{xy}^2 & a_{xz}^2 & 2a_{xy}a_{xz} & 2a_{xz}a_{xx} & 2a_{xx}a_{xy} \\ a_{yx}^2 & a_{yy}^2 & a_{yz}^2 & 2a_{yy}a_{yz} & 2a_{yz}a_{yx} & 2a_{yx}a_{yy} \\ a_{zx}^2 & a_{zy}^2 & a_{zz}^2 & 2a_{zy}a_{zz} & 2a_{zz}a_{zx} & 2a_{zx}a_{zy} \\ a_{yx}a_{zx} & a_{yy}a_{zy} & a_{yz}a_{zz} & a_{yy}a_{zz}+a_{yz}a_{zy} & a_{yx}a_{zz}+a_{yz}a_{zx} & a_{yy}a_{zx}+a_{yx}a_{zy} \\ a_{zx}a_{xx} & a_{zy}a_{xy} & a_{zz}a_{xz} & a_{xy}a_{zz}+a_{xz}a_{zy} & a_{xz}a_{zx}+a_{xx}a_{zz} & a_{xx}a_{zy}+a_{xy}a_{zx} \\ a_{xx}a_{yx} & a_{xy}a_{yy} & a_{xz}a_{yz} & a_{xy}a_{yz}+a_{xz}a_{yy} & a_{xz}a_{yx}+a_{xx}a_{yz} & a_{xx}a_{yy}+a_{xy}a_{yx} \end{bmatrix}$$

With these rotation matrices, for each selected crystal cut, a new set of material constant matrices in (x, y, z) can be determined based on the material constants given in its original crystal coordinated (X, Y, Z):

$$[c']=[M][c][M]^T$$
$$[e']=[a][e][M]^T$$
$$[\varepsilon']=[a][\varepsilon][a]^T$$

For this study, we take advantage of the Crystal Rotation Calculator available at zephrasoft.com to perform the transformation and obtained the transformed matrices.

4. Modeling Consideration

Once the rotated material properties are determined, we then used a 3D COMSOL model of a two-port SAW sensor to characterize the wave propagation characteristics in these crystal cuts. For the crystal materials, we considered trigonal crystal materials Langasite and Lithium Niobate. For the IDEs, their finger width and spacing are set at 5 μm. To excite the transmitting IDTs, an impulse potential signal is applied to the electrodes in an alternating manner:

$$V_{i+}=\begin{cases}+0.5V, t\le 1ns \\ 0V, t\ge 1ns\end{cases}, \qquad V_{i-}=\begin{cases}-0.5V, t\le 1ns \\ 0V, t\ge 1ns\end{cases}$$

To get the output signal, the voltage at the receiver IDTs is obtained in the same alternating manner.

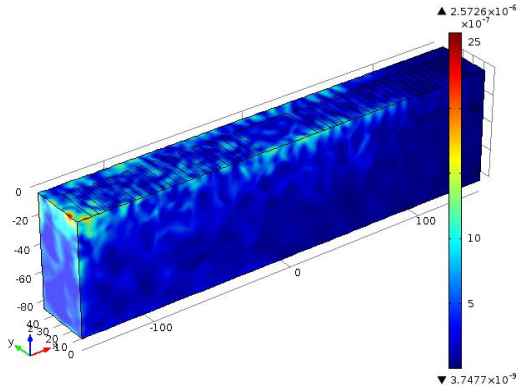

Fig. 3 – COMSOL model of a two-port delay line SAW sensor

The material properties matrices of Langaite are:

$$C_E=\begin{pmatrix} C_{11} & C_{12} & C_{13} & C_{14} & 0 & 0 \\ C_{12} & C_{11} & C_{13} & -C_{14} & 0 & 0 \\ C_{13} & C_{13} & C_{33} & 0 & 0 & 0 \\ C_{14} & -C_{14} & 0 & C_{44} & 0 & 0 \\ 0 & 0 & 0 & 0 & C_{44} & C_{14} \\ 0 & 0 & 0 & 0 & C_{14} & (C_{11}-C_{12})/2 \end{pmatrix}$$

$$e=\begin{pmatrix} e_{11} & -e_{11} & 0 & e_{14} & 0 & 0 \\ 0 & 0 & 0 & 0 & -e_{14} & -e_{11} \\ 0 & 0 & 0 & 0 & 0 & 0 \end{pmatrix}$$

$$\varepsilon=\begin{pmatrix} \varepsilon_{11} & 0 & 0 \\ 0 & \varepsilon_{11} & 0 \\ 0 & 0 & \varepsilon_{33} \end{pmatrix}$$

Langasite: (ϕ,θ, ψ) = (0°, 0°, 0°)	
C_{11}	18.89×10^{10} Nm^{-2}
C_{12}	10.42×10^{10} Nm^{-2}
C_{13}	10.15×10^{10} Nm^{-2}
C_{14}	1.44×10^{10} Nm^{-2}
C_{33}	26.83×10^{10} Nm^{-2}
C_{44}	5.33×10^{10} Nm^{-2}
e_{11}	-0.437 Cm^{-2}
e_{14}	0.104 Cm^{-2}
e_{31}	0.2 Cm^{-2}
ε_{11}	19.05
ε_{33}	51.81
ρ	5739 Kg m^{-3}

The material properties matrices of Lithium Niobate are:

$$C_E = \begin{pmatrix} C_{11} & C_{12} & C_{13} & C_{14} & 0 & 0 \\ C_{12} & C_{11} & C_{13} & -C_{14} & 0 & 0 \\ C_{13} & C_{13} & C_{33} & 0 & 0 & 0 \\ C_{14} & -C_{14} & 0 & C_{44} & 0 & 0 \\ 0 & 0 & 0 & 0 & C_{44} & C_{14} \\ 0 & 0 & 0 & 0 & C_{14} & (C_{11}-C_{12})/2 \end{pmatrix} \quad (5)$$

$$e = \begin{pmatrix} 0 & 0 & 0 & 0 & e_{15} & -e_{22} \\ -e_{22} & e_{22} & 0 & e_{15} & 0 & 0 \\ e_{31} & e_{31} & e_{33} & 0 & 0 & 0 \end{pmatrix} \quad (6)$$

$$\varepsilon = \begin{pmatrix} \varepsilon_{11} & 0 & 0 \\ 0 & \varepsilon_{11} & 0 \\ 0 & 0 & \varepsilon_{33} \end{pmatrix}$$

Lithium Niobate: (ϕ,θ, ψ) = (0°, 0°, 0°)	
C_{11}	20.3×10^{10} Nm^{-2}
C_{12}	5.3×10^{10} Nm^{-2}
C_{13}	7.5×10^{10} Nm^{-2}
C_{14}	0.9×10^{10} Nm^{-2}
C_{33}	24.5×10^{10} Nm^{-2}
C_{44}	6.0×10^{10} Nm^{-2}
e_{15}	3.7 Cm^{-2}
e_{22}	2.5 Cm^{-2}
e_{31}	0.2 Cm^{-2}
e_{33}	1.3 Cm^{-2}
ε_{11}	44
ε_{33}	29
ρ	4600 Kg m^{-3}

5. Results and Discussion

Since the SAW device we modeled has reciprocal and symmetric design for the two IDEs, i.e., S11=S22 (reflection coefficients) and S12=S21 (transmission coefficients), we quantified the insertion loss (-20log|S12|) for different crystal cuts.

$$IL = 20\times\log_{10}\left|V_{output}/V_{input}\right|$$

Moreover, we also determined the resonant frequency (f_0) from the modeling results and quantified the SAW travel velocity by using $v=\lambda f_0$, where λ is the wavelength of the generated SAW (λ=20 μm).

Fig.4 shows a typical series of output signals obtained at the receiver IDEs. With these measurements, the insertion loss spectra were determined by performing FFT. As shown in Fig.5 through Fig.8, insertion loss spectra of Langasite show that the SAW waves exhibit a resonant frequency from approximately 120 MHz to 135 MHz at different cut angles. With λ=20 μm, we estimate that the wave travels in a velocity around 2400 m/s to 2700 m/s in these Langasite cuts and propagation directions.

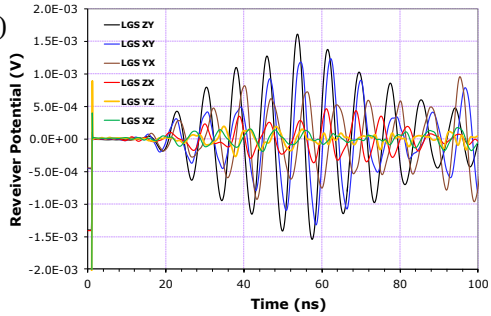

Fig. 4 – Time varying output signals obtained at the receiver IDEs.

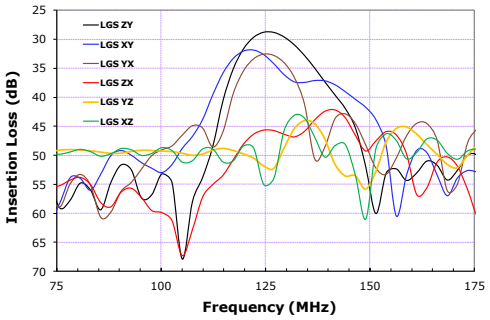

Fig. 5 – Insertion loss spectra of Langasite at various crystal cuts.

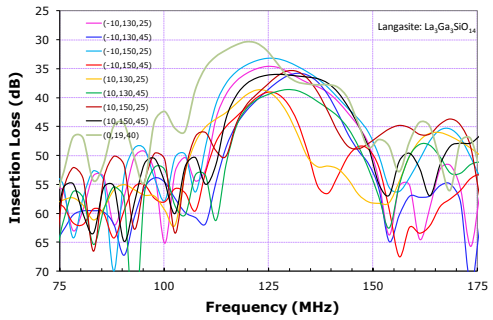

Fig. 6 – Insertion loss spectra of Langasite at various crystal cuts. Euler angles are specified in the legends.

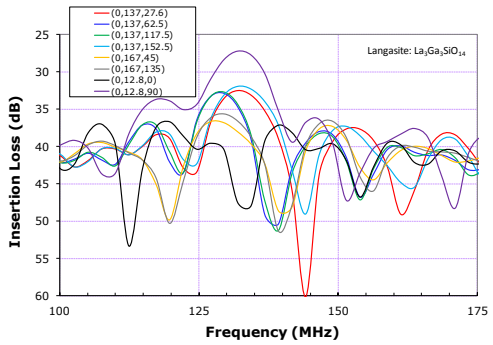

Fig. 7 – Insertion loss spectra of Langasite at various crystal cuts. Euler angles are specified in the legends.

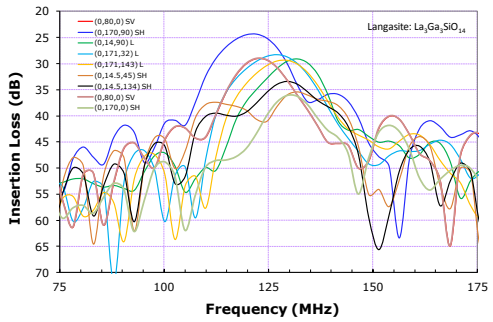

Fig. 8 – Insertion loss spectra of Langasite at various crystal cuts. Euler angles are specified in the legends.

Fig.9 shows the insertion loss spectra for Lithium Niobate substrate, where the resonant frequency is found from approximately 160 MHz to 190 MHz, which corresponds to a travel velocity of around 3200 m/s to 3800 m/s in these various crystal cuts and propagation directions.

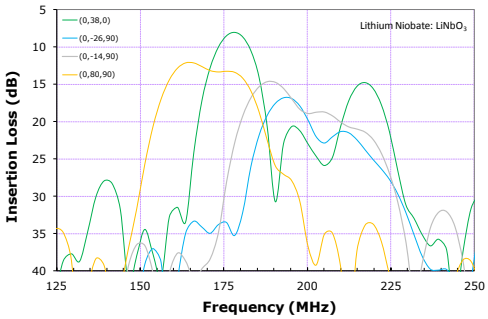

Fig. 9 – Insertion loss spectra of lithium niobate at various crystal cuts. Euler angles are specified in the legends.

6. Conclusions

This work not only reveals how insertion loss and SAW travel velocity are affected by the crystal cut angles and the wave propagation direction but also demonstrates that computer simulation can provide a better and cost-effective way to identify an optimal crystal orientation for the development of high performance SAW devices.

7. References

1. Yeswanth Rao and Guigen Zhang. 3D Modeling of a Surface-Acoustic-Wave Based Sensor, COMSOL Conference 2007, Boston, MA.
2. Guigen Zhang. Nanostructure-Enhanced Surface Acoustic Waves Biosensor and Its Computational Modeling, Journal of Sensors doi:10.1155/2009/215085
3. Daniel Royer and Eugen Dieulesaint. Elastic Waves in Solids I, Springer, 2000.

8. Acknowledgements

1. Institute for Biological Interface of Engineering at Clemson University
2. Advanced Computational Resources, Clemson Computing and Information Technology
3. zephrasoft.com for making available the Crystal Rotation Calculator